Combined effect of coal chemical wastewater and PC on preparing of coal-to-liquids residue-based alkali activated materials

Huimei Zhu[a], Hui Li[a,] *, Xudong Ma[a], Feng Wu[a], Qizhi Zhou[b], Yun Bai[b,] *

[a]*College of Materials Science and Engineering, Xi'an University of Architecture and Technology, Xi'an 710055, China*

[b]*Department of Civil, Environmental and Geomatic Engineering, University College London, London WC1E 6BT, the United Kingdom*

Abstract: Aimed to achieve "waste control by waste" of coal-to-liquids (CTL) industry, coal gasification residue (CGR), the most typical CTL residue, and coal chemical wastewater (CCW) were used as aluminosilicate precursor and auxiliary activator respectively to prepare alkali activated materials (AAMs). CGR-based AAMs using a less concentrated NaOH solution than conventional, with CCW as mixing water were synthesized. The results showed that CCW benefited the compressive strength of CGR-based AAMs significantly, but demonstrating slight reduction over time. The combined effect of CCW and Portland cement (PC) supplied continuous increase of strength and eliminated the strength reduction with age. The mechanisms behind the improved performance of the AAMs due to the introduction of CCW and PC were discussed by XRD, FTIR, TG-DSC, MIP and ESEM. It was found that the increased alkali content due to the introduction of the CCW, supplied more extensive dissolution of active aluminosilicate and progressive geopolymerization of CGR. The coexistence of both N-A-S-H gel and C-A-S-H gel (originated from the introduced PC) in hardened AAM pastes reduced the proportion of pores larger than 100 nm to less than 30%, and provided denser structure.

Keywords: coal-to-liquids residue, coal gasification residue, coal chemical wastewater, AAMs, strength

1 Introduction

Coal-to-liquids (CTL) is an advanced clean technology which uses coal as the raw material to produce liquid fuel (gasoline, diesel, jet fuel, etc.) through a series of hydrogenation reactions under a high temperature and pressure environment facilitated by catalysts. In recent years, CTL has made great progress in the chemical industry, as well as in the combustion and reburning to reduce NOx (Xie et al., 2010; Li and Miao, 2019). Figure 1 shows a widely used CTL process for manufacturing liquid fuels in China. From the process, there are two types of wastes are generated, namely, coal chemical wastewater (CCW) and CTL residues, as indicated in the Figure.

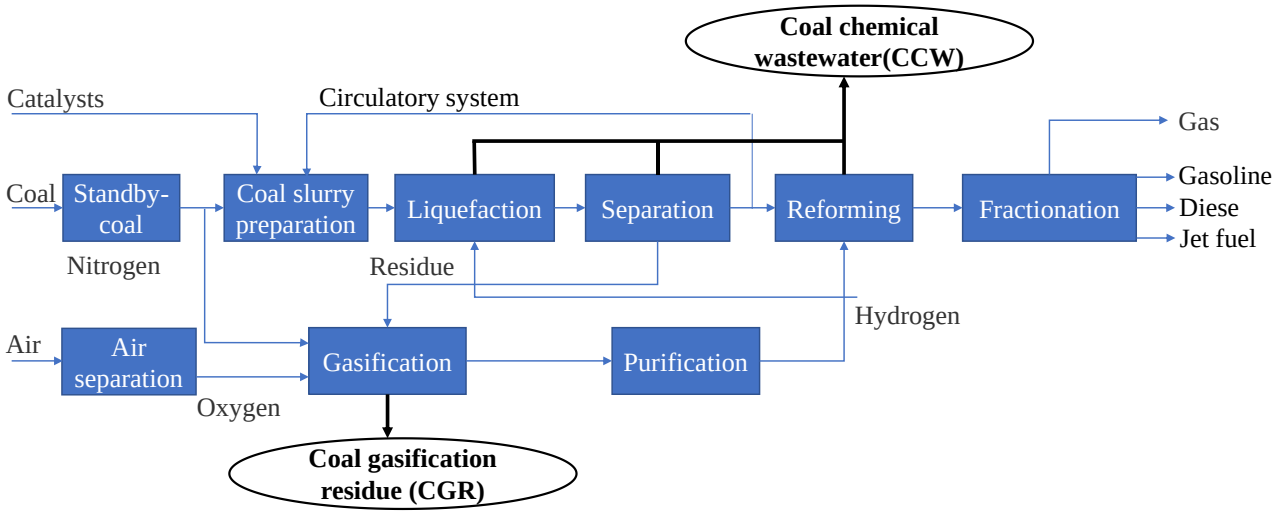

Fig. 1 The widely used CTL process in China and its main wastes

As shown in Fig. 1, the CTL residues are mainly generated during the coal gasification stage, hence, is often referred to as the coal gasification residue (CGR). The CGR usually includes coarse residue and fine residue (Aineto et al., 2006). The coarse residue refers to the part discharged from the bottom of gasifier through melting, quenching and condensation process under a high temperature (180~ 400°C depending on synthesis process and catalyst) and a high pressure (2~ 4 MPa). The carbon content of the coarse residue is relatively low (mostly lower than 5%), and the particle size distribution is 1~ 5 mm, accounting for 80% of the total CGR. The fine residue is carried by gas flowing through the top of the gasifier, and its carbon content is generally close to 30%. Approximately 1/3 of the particles of the fine residue are less than 80 μm, which accounts for about 20% of the total CGR. It was reported that more than 900,000 tonnes of CGR are produced in the CTL process with every one million tonnes of coal being processed (Xie et al., 2020). At present, the majority of CGR are stored at the landfill sites, causing serious environmental pollution and waste of land resources (Rani and Jain, 2014), which could offset the advantages brought by the clean development of CTL technology. To utilize the CGR, researches have been mainly on reusing the carbon in the CGR, especially its gasification reactivity (Zhao et al., 2010; Zdeb et al., 2019). The composition and structural characteristics of CGR have also been studied and reported that the main components of CGR are silicon, aluminium, calcium, iron, magnesium and titanium (Matjie et al., 2008; Yuan et al., 2014; Wu et al., 2015). Since silicon, aluminium and calcium are the main elements needed to form cementitious materials; the potential of producing cementitious materials with CGR has also been explored. For example, Li et al. (2019b) found that CGR could contribute to the cementitious reaction by forming ettringite, okenite and even C-S-H gel in CGR/cement blends, indicating that CGR may possess some reactivity which can benefit the properties of cementitious materials.

On the other hand, a large quantity of CCW, which is mainly composed of Cl^-, Na^+ and SO_4^{2-} with pH >9, has been discharged from the liquefaction, separation and reforming processes of CTL (Li et al., 2020b). Due to its high salt concentration, the CCW is difficult to be treated. In practice, evaporation and crystallization are used methods

for treating this wastewater. Although the salts obtained from these s processes can be used as raw materials in chlor alkali industry and soda ash industry and therefore can generate some added value (Gai et al., 2017; Liu et al., 2019), the process itself is too time-consuming and requires lots of resources, offsetting the added value. Some attempts have thus been made in the literature to use industrial wastewater as mixing water for manufacturing concrete in order to save natural water resources. However, it has been reported that some inorganic and organic compounds in industrial and domestic wastewater could hinder the hydration process of cement, and prolong its initial and final setting times (Babu et al., 2018). Nonetheless, the setting time of the cement paste prepared with some wastewater could still meet the limit requirements of ASTM and BS standards (Asadollahfardi et al., 2016, 2019). Additionally, Kaboosi et al. (2009) also indicated that the treated industrial wastewater at low concentrations can be used satisfactorily in the production of plain concrete.

Drawing upon the previous research reported in the literature on utilizing wastewater in concrete, at the same time, considering the potential pozzolanic property of CGR and the alkalinity of CCW (pH>9), alkali-activated materials (AAMs), formulated with alkaline activator and industrial by-products as an aluminosilicate precursor (Izquierdo et al., 2009; Provis et al., 2018), could provide an effective approach to the possible full recycling of CGR and CCW. Previous researches show that, in addition to their low energy consumption, AAMs also have some properties superior to Portland cement (PC), making it more suited for use in the repairing work (Gomaa et al., 2020; Zhang et al., 2020), nuclear waste immobilisation (Gijbels et al., 2018), high-temperature exposure (Çelikten et al., 2019) and multifunctional materials (Tang et al., 2019). Preliminary work carried out by Chen et al. (2019) proved that CGR can be blended with steel slag and incorporated into AAMs owing to its amorphous content. On the other hand, several researches on developing AAMs using seawater as mixing water have reported that the ions (Ca^{2+}, Cl^-, SO_4^{2-}, CO_3^{2-}, et al) in seawater could significantly contribute to the alkali-activation process (Ines et al., 2010; Rashad et al., 2013; Shi et al., 2019). Therefore, theoretically, the ions, such as Cl^-, Na^+ and SO_4^{2-}, existing in the CCW could also be able to contribute to the activation of CGR (Ahmed et al., 2018; Zhang et al., 2019).

In summary, the above literature review indicates that using CGR and CCW to produce AAMs could be a potential way to address the environmental issues caused by CTL and eventually contributing to the circular economy strategy of CTL technology. At the same time, this can also solve the raw materials shortage of AAMs. Therefore, in this study, the CCW was used as mixing water whilst the CGR was employed as an aluminosilicate source to manufacture AAMs. To further improve the strength of the AAMs by increasing calcium content, 10% of the CGR was also replaced by Portland cement. The AAMs manufactured with CGR and CCW were then characterized by compressive strength test, X-ray diffraction, FTIR and microstructure studies. Based on the results obtained, the mechanisms behind the improved performance of the AAMs due to the introduction of CCW and PC are then proposed and discussed in this paper.

2 **Materials and methods**

2.1 Materials

The CGR and CCW used in this study were obtained from a CTL plant in North-West of China. A Portland cement (PC), P.O 42.5, conforming to GB175-2007 and a reagent grade sodium hydroxide (NaOH) to initiate AAMs reactions were sourced locally. The chemical composition of the CGR and PC determined by X-ray fluorescence (XRF) are presented in Table 1. As can be seen, the CGR mainly consists of silica, alumina and lime with their contents being 49%, 20% and 11%, respectively. After grinding in the laboratory, the surface area of the CGR was 380 m^2/kg and its average particle size determined using Laser particle size analyzer LS230 was 22.08 μm. The XRD pattern of the CGR in Fig.3 shows that the CGR mostly consists of crystal quartz (SiO_2) and some amorphous phases as indicated by the hump between 15~ 40° (2θ). Additionally, the morphology of the CGR particles, as observed under Scanning Electron Microscope (SEM), revealed some diverse features, including round, flat and polyhedral shapes. On the other hand, the CCW mainly consists of chloride, sulfate and sodium ions with a pH value of 9.6. The SEM image and the particle size distribution of the CGR as well as the chemical composition of the CCW are given in the supplementary document.

Table 1 Chemical composition of the raw materials (wt. %)

Compositions	PC	CGR
SiO_2	21.78	48.75
Al_2O_3	4.21	20.05
CaO	60.88	10.69
Fe_2O_3	2.77	9.67
MgO	2.51	2.84
Na_2O	0.80	1.65
K_2O	0.91	2.11
TiO_2	0.80	1.01
SO_3	2.87	0.56
LOI	2.05	1.87

2.2 Specimen preparation

The batch mix proportions (employed in this study) of the CGR-NaOH system (T1, i.e. Control Mix), the CGR-NaOH-CCW system (T2), the CGR-NaOH-PC system (T3) and the CGR-NaOH -CCW-PC system (T4) are shown in Table 2. The raw materials were mixed in a NJ 160A mixer and the cube samples were cast in 20 ×20 ×20 mm molds which were subsequently cured at 80°C under steam for 24 hrs. Followed by this, the hardened specimens were cooled down to room temperature and then demolded before being cured under an ambient condition at (23±2) °C/ (90±5) %RH for 3, 7 and 28 days until being tested, respectively.

Table 2 Batch mix proportion (mass, g)

Samples	CGR	NaOH	PC	Tap water	CCW
T1	100	5	0	42	0
T2	100	5	0	0	42
T3	90	5	10	42	0
T4	90	5	10	0	42

2.3 Test methods

Compressive strength of the cube samples was measured at the age of 3, 7 and 28 days according to the Chinese Standard JGJ/T 70-2009. At each age, three samples were crushed and the average value was reported as the compressive strength.

The phase composition of the powders with particle size less than 80 μm was identified by a powder X-ray diffraction method (D/max 2200VB3+/PC, Rigaku International Corporation, Japan). The measuring speed was at 5° (2θ)/min in the 2θ range of 5~ 80°.

Fourier transform infrared (FIIR) spectra of the ground hardened pastes were collected using a FTIR Spectrometer Nicolet iS10 with a KBr beam splitter between the wavenumber of 500~ 4000 cm^{-1}.

The thermal stability of the AAMs was tested through TG-DSC (TGA/DSC1/1600). The test parameters were set as follows: scanning temperature range of 50~ 1000°C, heating speed of 20 °C/min with N_2 as the protective atmosphere.

Mercury Intrusion Porosimetry (MIP) with a MK-Auto Pore IV 9510 mercury porosimeter was used to investigate the pore distribution of the hardened AAM samples. The working pressure was 414 MPa and the measuring range was 30 Å~ 1000 μm.

The microstructure of the hardened AAM samples was observed using a ZEISS Gemini SEM 300 field emission scanning electron microscope (SEM). Sample surface was coated with gold and the observation was undertaken under a magnification range of 2000~ 30000 times.

3 Results

3.1 Compressive strength

The compressive strengths of the CGR-based AAMs cured for 3, 7 and 28 days are shown in Fig. 2. It can be seen that with the CGR being used as a precursor material, AAM mixes could be formulated, albeit the compressive strength of T1 (formulated with tap water) was quite low. This indicates that the aluminosilicates in the CGR can chemically involve in the geopolymerisation reaction of the AAM and be able to contribute to its strength. Additionally, when the CCW was used to replace tap water, the compressive strength of the CGR-based AAM was significantly increased compared to their counterparts with/without PC, respectively, at all the curing ages. This indicates that the CCW can promote/accelerate the chemical reaction of CGR-based AAMs and hence increased compressive strength. The increasing of strength could be presumably attributed to the increased alkali content due to the introduction of the CCW, even though the ions in the CCW could have also contributed to the reaction. However, in the absence of PC, the compressive strength of the AAM mixed with both tap water and the CCW (i.e. Mixes T1 and T2) exhibited slight reduction at the age of 28 days, for example, from 16.3 MPa at 7 days to 13.9 MPa at 28 days for Mix T2. As the CGR mainly consists of silica and alumina, it is anticipated that the main reaction products should be sodium aluminosilicate hydrate (which is also confirmed by the FTIR results and further discussed

below). As reported in the literature (Fernández-Jiménez et al, 2005; Sindhunata et al, 2008), the reduction of the compressive strength in AAMs over time could be the result of the continued polymerization of the sodium aluminosilicate hydrate (N-A-S-H) gel which could lead to the formation of further densified gel and, hence, increased porosity and reduced strength. On the contrary, when 10% of the CGR was replaced by PC, not only was the compressive strength increased as compared to their counterparts with/without the CCW, respectively, but the strength reduction was also eliminated. Additionally, using CCW as mixing water in Mix T4, the compressive strength further increased at all the curing ages as compared to Mix T3 which was mixed with tap water. It has been reported that the coexistence of N-A-S-H and calcium aluminosilicate hydrate (C-A-S-H) gels can eliminate the strength reduction of AAMs and promote the long-term strength gain due to the continued formation of C-A-S-H gel (Kumar et al, 2010). The improved strength performance of T3 and T4 could, thus, be the results of the coexistence of N-A-S-H and C-A-S-H gels in the AAMs as confirmed by the FTIR results below.

To identify the quantitative effects that the CCW and PC may have on the compressive strength of the CGR-based AAMs, the relative compressive strengths of Mixes T2, T3 and T4 (relative to the compressive strength of Mix T1 at each age, respectively) are presented in Table 3. It can be seen that the compressive strength of the CGR-based AAMs was improved by more than 100% when the CCW was used as the mixing water (Mix T2) as compared to using tap water (Mix T1). In contrast, with 10% of the CGR replaced by PC (Mix T3), the AAM mixed with tap water exhibited less increase in compressive strength, which is only 8~ 45% higher than that of the control specimen (Mix T1). However, it should be noted that compared with the compressive strength at 3 and 7 days, PC eliminated the strength reduction at 28 days.

More importantly, the combined effects of the CCW and PC (as revealed in Mix T4) on the compressive strength of the CGR-based AAM are extremely noticeable. The strength enhancing rates of the CGR-based AAM at the age of 3 and 7 days are more than 200%, and the strength raising rate at 28 days is even as high as 462% times compared to that of the Mix T1.

The above results showed that the combined application of the CCW and PC not only can greatly improve the compressive strength of AAMs, especially at 28 days, but can also eliminate the strength reduction. In the following sections, the mechanism of individual and combined effects of the CCW and PC on the strength behavior of the CGR-based AAMs are further investigated and discussed.

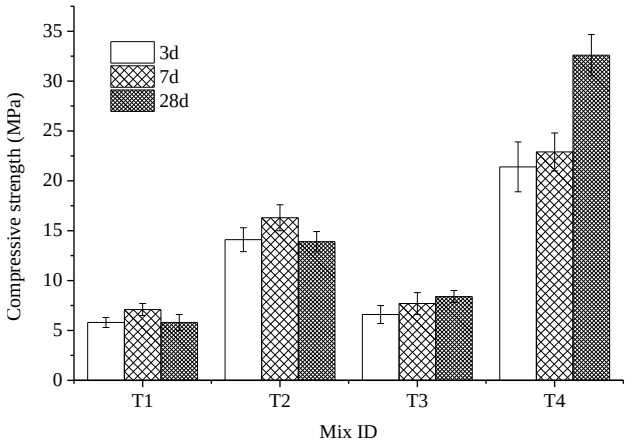

Fig. 2 Influence of the CCW and PC on the compressive strength of the CGR-based AAMs

Table 3 Effects of the CCW and PC on the relative compressive strength of the CGR-based AAMs (%)

Mix ID	Influencing Factor	Relative Compressive Strength (%)		
		3 days	7 days	28 days
T2	CCW	143.1	129.58	139.66
T3	PC	13.79	8.45	44.83
T4	Combined effect of CCW and PC	268.97	222.54	462.07

3.2 X-ray diffraction

The cementitious properties of AAMs are predominantly provided through the geopolymerization, which refers to the chemical reaction between "Si-O-" and "Al-O-" after the "Si-O- Si" and "Al-O- Al" in the raw materials are broken down by strong alkaline when the OH^- dissolved in water. This is then followed by the polycondensation of the dissolved phases (Izquierdo et al., 2009). The geopolymerization products formed in the CGR-based AAMs at the age of 28 days, together with the CGR, were characterized by XRD in the region of 10^o~ 50^o (2θ), and are shown in Fig. 3. It is evident that the CGR mostly consisted of quartz (i.e. crystalline SiO_2) and amorphous phase as indicated by a hump at around 15^o~ 40^o. The quartz and iron from the CGR were the main crystalline phases identified in the control AAM (i.e. Mix T1). In addition, the hump of the CGR in Mix T1 significantly decreased, which indicates that the aluminosilicates in the amorphous phases of the CGR might have involved in the geopolymerization reaction with sodium hydroxide. This again implies that the CGR is chemically reactive and can effectively contribute to the formation of AAMs.

On the other hand, in the AAM formulated with the CCW (i.e., Mix T2), additional calcium silicate hydrate C-S-H(I) with low Ca/Si ratio was detected, indicating that the introduction of the CCW can further enhance the chemical reaction. This could be attributed to the increased alkalinity by the CCW which might have increased the break-down of Si-O bonds in the CGR (because Si-O bond is stronger than the Al-O bond) (Ismail et al., 2009), leading to the precipitation of C-S-H (I). Moreover, a crystalline phase of halite (NaCl) from the CCW is also remarkable in the XRD pattern of Mix T2, which could be the results of the precipitation of NaCl from the Cl ions

existing in the CCW (as shown in the chemical analysis of the CCW in the Supplementary document). When 10% CGR was replaced by PC (Mix T3), the C-S-H(I), C-A-H gel and C-A-S-H gel were detected. Compared to Mix T1, it can be seen that more C-S-H (I) was formed. It is usually anticipated that the hydration of PC should form C-S-H (II) with a higher Ca/Si (Gard and Taylor, 1976.). The formation of additional low Ca/Si C-S-H (I) gel indicates that the introduction of PC into the CGR-based AAMs can further promote the dissolution of the CGR and hence increase the amounts of silica, leading to the formation of low Ca/Si C-S-H (I). Similarly, it seems that the formation of C-A-H and C-A-S-H gels could be attributed the calcium from PC as well as calcium released from CGR enhanced by PC. Furthermore, under the combined action of the CCW and PC (i.e. Mix T4), the intensity of the C-S-H (I) peak is further increased which could be attributed to the extra alkalis provided by the CCW and, hence, the increased formation of C-S-H(I).

It should be noted that while the hydration products like C-S-H(I), C-A-H and C-A-S-H can be identified in XRD, the geopolymerisation product, N-A-S-H gel, cannot be recognized by XRD. However, N-A-S-H gel can be clearly identified by FTIR which will be discussed in the following section, demonstrating the hydration of CGR-based AAM is further promoted. Meanwhile, some peaks referring to the complex salts of magnesium and chlorine or sulfate appeared at 33°~ 35° (2θ) in the XRD pattern of Mix T4. This could be due to the reaction between the magnesium ions from the CCW and/or released from the CGR with the chloride ions in the CCW. Overall, from the above results, it can be tentatively concluded that both the CCW and PC can promote the chemical reactions of AAMs In particular, the combination of the CCW and PC shows greater effect in promoting these reactions than the individual effect of each.

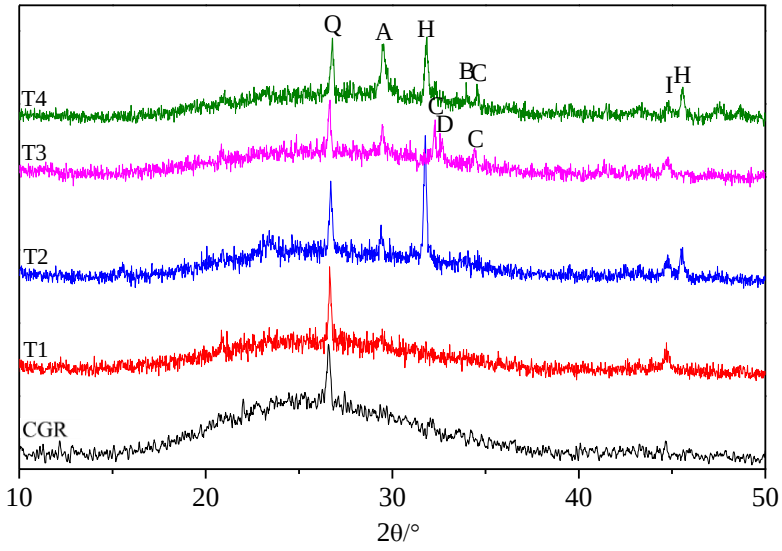

A: C-S-H(I)($CaO{\cdot}SiO_2{\cdot}H_2O$); B: Magnesium chloride hydroxide hydrate ($Mg_3(OH)_5Cl_4{\cdot}H_2O$); C: C-A-H($Ca_4Al_2O_7{\cdot}19H_2O$); D: C-A-S-H ($Ca_3Al_2(SiO_4)(OH)_8$); Q: quartz ($SiO_2$); I: Iron; H: Halite (NaCl).

Fig. 3 XRD patterns of CGR-based AAMs at age of 28 days

3.3 Fourier transform infrared spectroscopy

The FTIR spectra of the raw CGR particles and the CGR-based AAMs cured for 28 days are shown in Fig. 4. It is evident that the band in the region of 3400~ 3500 cm^{-1} due to stretching vibrations of O-H groups in H_2O or hydroxyls and the band centered around 1600 cm^{-1} due to the H-O-H bending vibration of molecular H_2O can be clearly identified in all the samples. The typical bands of the asymmetric stretching vibrations of C-O bonds were also observed at 1300~ 1400 cm^{-1}. Most importantly, it can be seen that the band centered at 1096 cm^{-1} in the raw CGR due to the asymmetric stretching vibration of T-O-Si (T=Al or Si) becomes sharper and shifted to the lower frequencies (996~ 1011 cm^{-1}) in the Mixes T1-T4, which could be attributed to the formation of the amorphous N-A-S-H gels (Garcı´a-Lodeiro et al., 2008). Especially, compared to Mix T1, this band becomes even sharper when tap water was replaced by the CCW in Mix T2, indicating an increased formation and enhanced geopolymerisation of the N-A-S-H gels. In contrast, when 10% of the CGR was replaced by PC in both Mixes T3 and T4, the band associated to the N-A-S-H gel became flatter and broader. Actually, even in the case of Mixes T1 and T2, shoulder at around 1100 cm^{-1} could also be identified. It has been reported that the addition of Ca into the N-A-S-H can not only modify the N-A-S-H gel, but may also lead to the formation of C-A-S-H gel. In particular, at high pH (>12), the presence of Ca may even degrade N-A-S-H in favour of the formation of C-(A)-S-H gel (Walkley et al., 2016). In the current study, the CGR contains around 10% CaO. In addition, 10% CGR was replaced by PC (which contains around 60% CaO). Therefore, the increased broad nature of the band between 900~ 1200 cm^{-1} could be the consequence the combined effects of N-A-S-H and C-(A)-S-H gels. Previous research has shown that by deconvoluting the spectra in this wavenumber range, the C-(A)-S-H gel can be clearly distinguished from the N-A-S-H gel (Garcı´a-Lodeiro et al, 2008). The peak fitting was, thus, adopted in the current research to acquire a better understanding of the products formed in the CGR-based AAM pastes. The wavenumber and the respective area of each of the band identified from the deconvolution of the main band between 900~ 1200 cm^{-1} are shown in Fig.5 and Table 4.

As can be seen in Fig. 5, two components, represented by band 1 and band 2 at 986~ 999 cm^{-1} and 1073~ 1099 cm^{-1}, were clearly revealed after the deconvolution of the main band between 900~ 1200 cm^{-1}. It has been widely accepted that when the C-(A)-S-H and N-A-S-H gels co-existed in a system, the Si-O stretching band in the C-(A)-S-H gel should be centered at around 975 cm^{-1} (when Ca/Si ratio is 1), whilst the N-A-S-H gel at around 1006 cm^{-1} (when Si/Al ratio is 1). Therefore, the band 1 and band 2 identified in Fig. 5 are associated to the C-(A)-S-H and N-A-S-H, respectively. Additionally, it can be observed that the band corresponding to T-O (T = Si or Al) stretching vibrations in the C-(A)-S-H gel shifted toward higher wavenumbers, namely from 986 cm^{-1} (T1), to 992 cm^{-1} (T2), 997 cm^{-1} (T3), 999 cm^{-1} (T4). This indicates that the Ca/Si ratio decreases from T1 to T4, which could be attributed to the progressive polymerization of silicates chains (Yu et al., 1999). On the other hand, the associated band in the

N-A-S-H gel also shifted toward higher wavenumbers, namely from 1073 cm^{-1} (T1), to 1086 cm^{-1} (T2), 1091 cm^{-1} (T3), 1099 cm^{-1} (T4), indicating an increase in Si/Al ratio from T1 throughout to T4 which could be possibly due to the progressive polymerization of aluminosilicates (Yip and Deventer, 2003). Furthermore, from Table 4, it can be seen that by integrating the area of band 1 of these four mixes, some interesting features can be observed: the CCW increased the proportion of the C-(A)-S-H gel from 23.13% to 39.5% when the tap water in Mix T1 was replaced by the CCW, indicating that the CCW could enhance the activation of the CGR and, thus, promoted the chemical reaction between calcium and reactive aluminosilicate released from the CGR. PC further increased the proportion of C-(A)-S-H gel due to its hydration, and the improvement of CCW and PC are superimposed when they are combined. Ismail et al. found that C-S-H gel coexisting with N-A-S-H gel resulted in higher compressive strength with slag addition in alkali activated fly ash system, so it can be concluded that C-(A)-S-H gel plays an important role in eliminating the strength reduction of CGR-based AAMs at 28 days in this study.

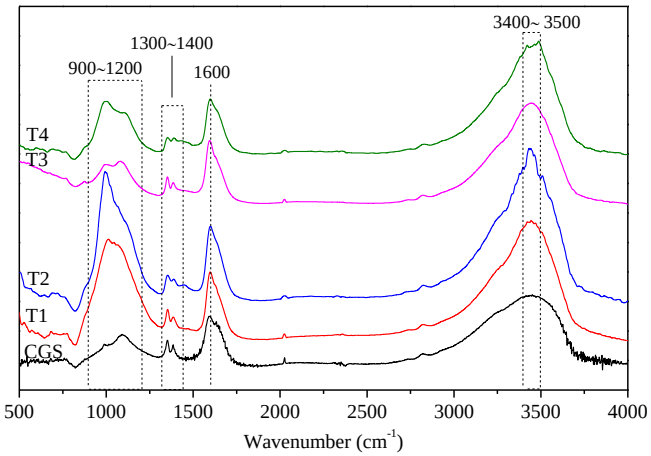

Fig. 4 FTIR spectra of CGR -based AAMs at age of 28 days

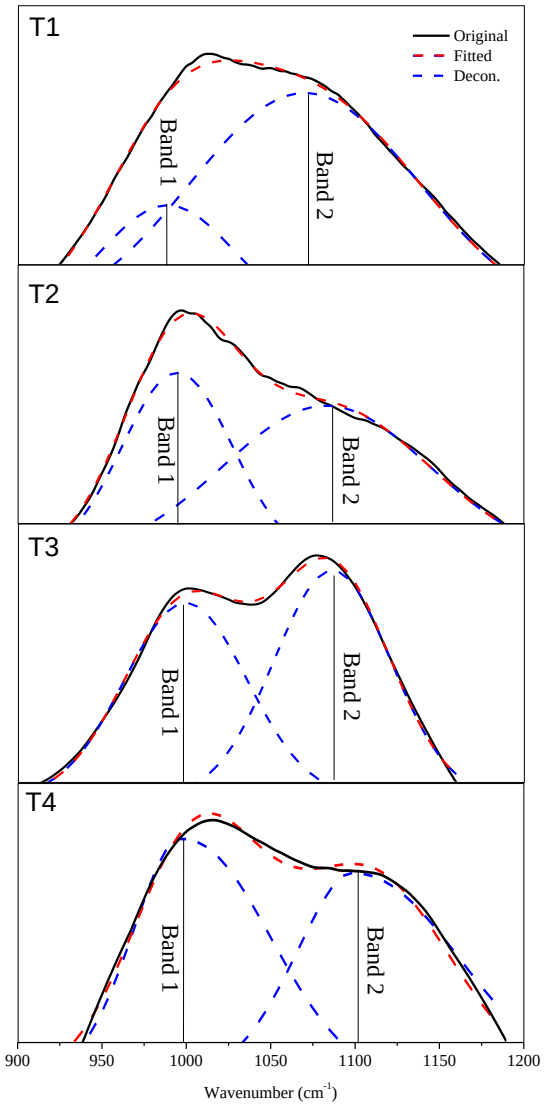

Fig. 5 DE convolution of selected FTIR spectra (900~1200 cm^{-1}) in Fig. 4

Table 4 Bands fitted and their integral intensity showed in Fig.7 (%)

Bands	T1		T2		T3		T4	
	V(cm^{-1})	Area (%)	V(cm^{-1})	Area (%)	V(cm^{-1})	Area (%)	V(cm^{-1})	Area (%)
Band 1	986	23.13	992	39.51	997	44.27	999	57.08
Band 2	1073	76.87	1086	60.49	1091	55.73	1099	42.92
Area (band 1)/area (band2)	0.3		0.65		0.79		1.33	

3.4 Differential thermogravimetry

The differential thermograms (DTG) patterns of CGR-based AAMs are shown in Fig. 6. The characteristic peak below 200 ºC (R1) represents the release of physically bound water in the gel structure (mainly in the pore network) (Alarcon-Ruiz et al., 2005). Using CCW as the mixing water, the peak in this temperature range become sharper and the corresponding mass loss rate calculated from the TG curves increased from 3.14% (Mix T1) to 5.16% (Mix T2) and 5.83% (Mix T4) respectively, as shown in Table 5, meaning again that CCW promoted the formation of gels in CGR-based AAMs. When CGR was replaced by 10% PC, Table 5 shows a weight loss corresponding to

decomposition of Ca(OH) (R2 in Fig. 6), a common hydration product of PC, increased from 1.22% (Mix T3) to 1.77% (Mix T4)

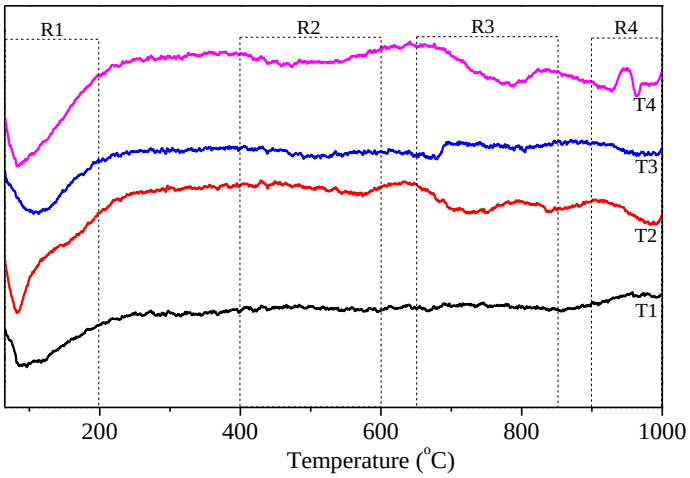

Fig. 6 DTG patterns of CGR-based AAMs.

Table 5 Peaks attributions on the DTG patterns and mass loss rates of CGS-based AAMs

Region	Temperature /°C	Attribution	Mass loss rates (%)			
			T1	T2	T3	T4
R1	below 200	Evaporation of hydrate water	3.14	5.16	3.67	5.83
R2	400~ 600	Decomposition of Ca $(OH)_2$	0.57	0.87	1.22	1.77
R3	650~ 850	Decomposition of calcite	0.54	2.09	0.82	2.31
R4	850~ 1000	Crystallization of gels	0.125	2.01	0.74	2.58

3.5 Pore size distribution by mercury intrusion porosimetry

The pore size distributions of CGR-based AAMs at age of 28 days are shown in Fig. 7. It is well recognized that the pore size of hardened cement paste can be divided into four grades, namely, gel pores (<10 nm), transition pores (10~ 100 nm), capillaries (100~ 1000 nm) and macropores (>1000 nm) (Kaufmann, 2004). The cumulative pore volume of samples in this study according to the above classification is shown in Table 6.

When mixed with CCW, the cumulative pore size of Mix T2 decreased sharply, from 40.88% to 17.25% compared with the control AAM (Mix T1). While the proportions of transition pores and capillaries remained similar to that of the control specimen, the capillary pores shifted toward smaller pore diameter (Fig.7) . The major changes observed was increasing of the gel pores (from 6% to 13.35%) and reducing of the macropores (from 20.92% to 9.28%). As revealed by XRD and FTIR results, the CCW promoted the polymerization of CGR to form more gel, the pores plugging effect of precipitated chloride (Janina et al., 2008), leading to the reduction of total porosity in AAMs. However, the main reaction product of CGR-based AAM mixed with CCW is dominated by N-A-S-H (confirmed by FTIR), which brings a large number of transition pores and capillaries (Sindhunata et al, 2008).

Although PC alone has little effect on the cumulative porosity of AAMs, Mix T3 shows largely increasing the proportion of transition pores and reducing the proportion of capillaries and macropores, Its pore size distribution curve shows a doublet feature, (Xie et al, 2019). With combined effect of PC and CCW (Mix T4), the doublet feature

of PC is still visible but shifts further towards smaller pore diameter in the Fig 7, while the peak between 100nm and 1000nm significantly reduces. This is mainly attributed to the higher proportion of C-(A)-S-H gel formed and gradually densified with aged (Bahafid et al, 2014) as shown by the XRD and FTIR results. Mix T4 developed the smallest average pore size (15.2 nm), the largest gel pore ratio (27.11%) and the smallest capillary ratio, making it the optimal of the four mixes. As gels are main strength given component in PC both PC hydration products and AAM products, the pore size distribution results well explain the compressive strength results reported in section 3.1 as well as by other researchers (Li et al., 2019a; Hu et al., 2020).

Additionally, the reducing of pore size to form dense gel products could greatly reduce permeability of AAMs, therefore increase immobilization of hazardous substances originated from the waste raw materials, such as CGR and CCW.

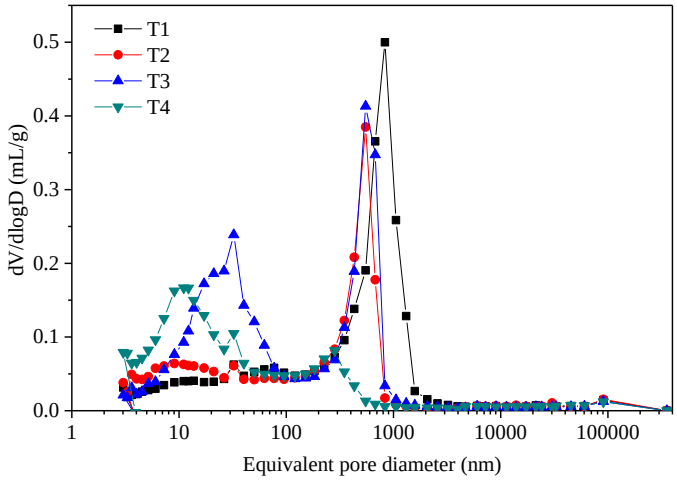

Fig. 7. Pore size distribution of CGR-based AAMs at age of 28 days

Table 5 Total porosity and pore size distribution of AAMs

Sample	Porosity /%	Average pore diameter /nm	Pore size distribution/%			
			<10 nm	10~100 nm	100~1000 nm	>1000 nm
T1	40.88	57.7	6	16.24	56.84	20.92
T2	17.25	30	13.35	22.5	54.87	9.28
T3	42.70	33.7	7.58	44.06	42.23	6.13
T4	32.90	15.2	27.11	43.2	21.34	8.33

3.6 Scanning electron microscopy

Fig. 8 shows the micromorphological characteristic of CGR-based AAMs pastes at 28 days. Further enlarged images (x 30,000) with detailed features are displayed in Fig 9, while Fig 9(a) and Fig 9(b) focus on unreacted and reacted CGR particles respectively. In Fig 8, for the control sample (Mix T1) a large number of unreacted CGR particles can be observed, together with the reaction products scattered on the surface of or formed between unreacted CGR particles. When CCW used as mixing water (Mix T2), the surface of CGR particles was corroded, showing lots of hollows due to dissolution of active aluminosilicate components, illustrated by XRD and FTIR results earlier. Signs of reaction can be observed on the surface of CGR particle (Mix T2 in Fig 9(a)) and the formed porous gels

are denser than the control sample (Mix T2 in Fig.9(b)). When 10% PC replacement was added, majority CGR particles were reacted, mostly wrapped by reaction products layers (Mix T3) as demonstrated in Fig.8. Different from the CGR particles in the control sample, the CGR surfaces in Mix T3 were covered by the agglomerates of adhesion products. Moreover, the connection between reaction products became denser because of the hydration of PC and formation of C-A-S-H gel, which is consistent with the results of MIP and FTIR. Under the combined effect of CCW and PC, the micromorphology of AAM shows the geopolymerisation was further advanced, that is, the gels were more compact and the corrosion on the surface of CGR particles were more intensive (Mix T4 in Fig.9), indicating the reaction of CGR raw material was promoted significantly.

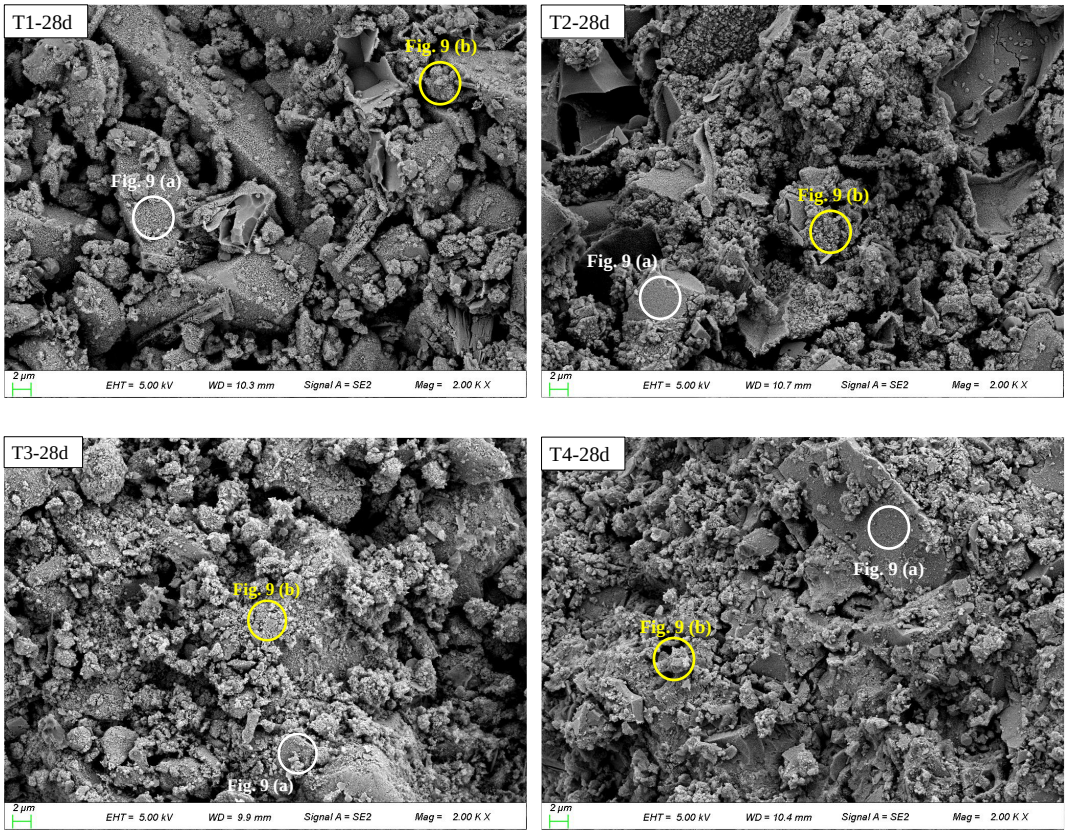

Fig. 8. SEM images of CGR-based AAMs at age of 28 days

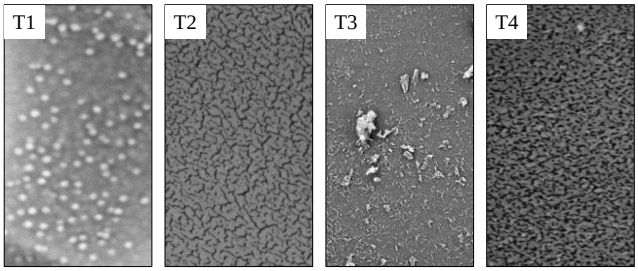

(a)

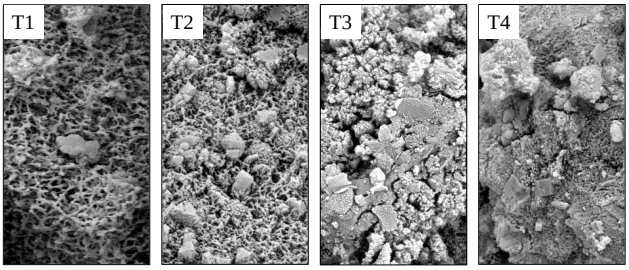

(b)

Fig. 9. SEM images of (a) CGR particles surface and (b) reaction products with the magnification at 30,000 times

4 Discussions

Abundant research has been done on the synthesis of AAM using industry residues containing active aluminosilicate as precursor material. This study is a feasibility study and –confirms that CGR from CTL technology has latent chemical activity and can be involved in the geopolymerisation reaction with alkali activators. XRD results show that the amorphous phase hump around 15^{o}~ 40^{o} (2θ) in CGR decreased obviously in the XRD pattern of the CGR-NaOH AAM paste through the polymerization between the amorphous phase in the CGR and alkali activators.

CCW form the same CTL technology can be used as an auxiliary activator together with the less concentrated NaOH solution to stimulate the activity of CGS. Three reasons can be concluded: (i) Alkalinity from CCW results in faster and more extensive dissolution of active silicon and aluminum than tap water, especially the Si-O bonds with higher force constant in the CGR (Ismail et al., 2009), so that a higher extent and degree of geopolymerization takes place (as shown by XRD and FTIR results), leading to the generation of more geopolymeric N-A-S-H gel, which can also be obtained from SEM pictures. (ii) It was proved that the appropriate amount of sodium chloride (Guerrero et al., 2009) and sulfate (Deng et al., 2020) promoted the hydration of fly ash, accordingly, the dissolution and geopolymerization of CGR may be intensified under the effect of sodium chloride and sulfate in CCW. Both XRD and FTIR results indicate that the formation of C-S-H (I) with lower Ca/Si ratio is also promoted, and the higher surface areas of C-S-H phase with lower Ca/Si ratio was considered to contribute to the increase of compressive strength (Puertas and Fernández-Jiménez, 2003). (iii) Sodium chloride, rich in CCW, crystallizes and precipitates in the AAM pastes as shown by XRD analysis, which significantly decreases the total porosity of AAM pastes together with the formation of gels. In addition, for the optimal CGR-NaOH -CCW-PC system (Mix T4) in this manuscript, the influence of CCW on PC hydration cannot be ignored. It is well known that chloride plays a catalytic role with calcium oxychloride as the intermediate product to enhance the transport of calcium hydroxide, thus promoting the hydration of PC and the forming of dense C-S-H gel (Cheeseman and Asavapisit, 1999). Moreover, the rich sulfate in CCW also promotes the early hydration of PC, mainly due to that the rate of aluminate phase consumption was influenced significantly by the solubility of the sulphate (Tang and Glasser, 1988). All these

findings provide a basis for improving the application of CCW in cementitious materials and achieving "waste control by waste".

The strength development in conventional alkali-activated aluminosilicate binders such as Mix T1 and Mix T2 is provided by the formation of a three-dimensional N-A-S-H gel as the main reaction product. However, the continued polymerization of N-A-S-H gel could lead to the formation of further densified gel and, hence, increased porosity and reduced strength over time (Fernández-Jiménez et al, 2005; Sindhunata et al, 2008). The greatest significance of introducing PC into the CGR-based AAMs is to increase the Ca content within the reaction mixture and promote greater formation of C-A-S-H gels, thus forming the coexistence of both N-A-S-H and C-A-S-H gels, so as to eliminate the reduction of strength over time and improve the pore size distribution of hardened pastes. Although the viewpoint that the coexistence of N-A-S-H and C-A-S-H gels inevitably affects the properties and performance of AAMs has been proposed, the previous approaches to this problem mainly involved synthesis of AAM synthesized with laboratory reagents (Na_2O, CaO, Al_2O_3, SiO_2 and H_2O). In this study, the application of PC as calcium source additive in the CGR-NaOH-CCW system makes it possible to achieve "waste control by waste" for CTL technology in practice. Moreover, the C-A-S-H gel remained relatively unchanged compared with the N-A-S-H gel in the toxicity characteristic leaching procedure (Izquierdo ea al., 2009). So, the CGR-NaOH-CCW-PC system adopted in this manuscript provides an idea about precursor chemistry controls for inhibiting the leaching of contaminants.

5 Conclusions and prospect

Abundant research has been done on the synthesis of AAM using industry residues containing active aluminosilicate as precursor material. This study is a feasibility study and confirms that CGR from CTL process has latent chemical activity and can be activated by alkali activators to form AAMs. XRD results show that the amorphous phase hump around 15^o~ 40^o (2θ) in CGR decreased obviously in the XRD pattern of the CGR-NaOH AAM paste through the polymerization between the amorphous phase in the CGR and alkali activators.

CCW from the same CTL process can be used as an auxiliary activator together with a less concentrated NaOH solution to stimulate the activity of CGR. In addition, it benefits the compressive strength of CGR-based AAMs significantly, which could be attributed to faster and more extensive dissolution of active aluminosilicon and progressive geopolymerisation of CGR. However, the AAM with CGR-NaOH-CCW system shows slight strength reduction over time, as a result of the continued polymerization of N-A-S-H gel (the main reaction products in theses mixtures) leading to the proportion of pores larger than 100 nm more than 60% at 28 days.

When 10% of the CGR was replaced by PC, not only was the compressive strength increased, but the strength reduction was also eliminated. Especially, in the Mix using CCW and PC together, the compressive strength further increased noticeably at all the curing ages as compared to the mixture without PC. The strength development is

provided by the coexistence of both N-A-S-H gel and C-(A)-S-H gel (originated from the introduced PC) in hardened AAM pastes, and the continued formation of C-(A)-S-H gel reduces the proportion of pores larger than 100 nm to less than 30%. The refinement of C-A-S-H gel on the pore size distribution is not only conducive to the development of strength, but also expected to reduce the leaching of hazard contaminants.

This study confirms that using CGR and CCW, two wastes from the CTL process, to produce AAMs for construction industry could be a promising way to address the environmental issues caused by CTL, converting risk to resources. It could eventually contribute to the circular economy strategy of CTL technology.

This study shows that when CCW and PC added together, MMAs show significant improvement than added individually. Mathematical proof is needed to further understand the possible synergy of CCW and PC. Moreover, attention should also be paid on the long-time strength development and durability of the proposed CGR based AAMs. Due to the nature of reusing wastes as raw materials, the environment impact of CGR-based AAMs mixed with CCW should be investigated profoundly.

Acknowledgement

Financial supports from National Natural Science Foundation of China (51828201) and Natural Science Foundation of Shaanxi Province (2012JM6001) are greatly acknowledged.

References

Ahmed S. A., Metwally M.E.A., Zakey S.E., 2018. Utilizing industrial waste-water as alkali activator in sand-cement kiln dust bricks. Constr. Build. Mater. 182, 284-289.

Aineto M., Acosta A., Rincón J. Ma., Romero M., 2006. Thermal expansion of slag and fly ash from coal gasification in IGCC power plant. Fuel 85, 2352-2358.

Alarcon-Ruiz L., Platret G., Massieu E., Ehrlacher A., 2005. The use of thermal analysis in assessing the effect of temperature on a cement paste. Cem. Concr. Res. 35(3), 609-13.

Asadollahfardi G., Delnavaz M., Rashnoiee V., Ghonabadi N., 2016. Use of treated domestic wastewater before chlorination to produce and cure concrete. Constr. Build. Mater. 105, 253-261.

Asadollahfardi G., Mahdavi A.R., 2019. The feasibility of using treated industrial wastewater to produce concrete. Struct. Concrete 20, 123-132.

Bahafid S., Ghabezloo S., Duc M., Faure P., Sulem J., 2017. Effect of the hydration temperature on the microstructure of Class Gcement: C-S-H composition and density. Cem. Concr. Res 95, 270-281.

Babu G.R., Ramana N.V., 2018. Feasibility of wastewater as mixing water in cement. Mater. Today: Proceedings 5, 1607-1614.

Çelikten S., Sarıdemir M., Deneme I.O., 2019. Mechanical and microstructural properties of alkali-activated slag and slag + fly ash mortars exposed to high temperature. Constr. Build. Mater. 217, 50-61.

Chitsaz S., Tarighat A., 2020. Molecular dynamics simulation of N-A-S-H geopolymer macro molecule model for prediction of its modulus of elasticity. Constr. Build. Mater. 243, 118176.

Chen Y.Ch., Zhou X., Wan Sh., Zheng R., Tong J., Hou H.B., Wang T., 2019. Synthesis and characterization of geopolymer composites based on gasification coal fly ash and steel slag. Constr. Build. Mater. 211, 646-658.

Cheeseman C.R., Asavapisit S., 1999. Effect of calcium chloride on the hydration and leaching of lead-retarded cement. Cem. Concr. Res. 29 (6), 885-892.

Deng G., He Y.J., Lu L.N., Hu Sh.G.,2020. Evolution of aluminate hydrate phases in fly ash-cement system underthe sulfate conditions. Constr. Build. Mater. 252,119045.

Fernández-Jiménez A., Palomo A., Criado M., 2005. Microstructure development of alkali-activated fly ash cement: a descriptive model. Cem Concr Res.35(6),1204-1209.

Gard J.A., Taylor H.F.W., 1976. Calcium silicate hydrate (II) ("C-S-H(II)"). Cem. Concr. Res. 6, 667-677.

Garcia-Lodeiro I., Palomo A., Fernández-Jiménez A., Macphee D.E., 2011. Compatibility studies between N-A-S-H and C-A-S-H gels. Study in the ternary diagram Na_2O-CaO-Al_2O_3-SiO_2-H_2O. Cement Concrete Res. 41, 923-931.

Gai H.J., Feng Y.R., Lin K.Q., Guo K., Zhou H., 2017. Heat integration of phenols and ammonia recovery process for the treatment of coal gasification wastewater. Chem. Eng. J. 327, 1093-1101.

Janina K., Swiate G., 2008. No finite invariant density for Misiurewicz exponential maps. C. R. Acad. Sci. Paris, Ser. I. 346, 559-562.

Guerrero A., Goñi S., Allegro V. R., 2009. Durability of class C fly ash belite cement in simulated sodium chloride radioactive liquid waste: Influence of temperature. J. Hazard. Mater.162, 2-315, 1099-1102.

Gijbels K., Iacobescu R. I., Pontikes Y., Vandevenne N., Schreurs S., Schroeyers W., 2018. Radon immobilization potential of alkali-activated materials containing ground granulated blast furnace slag and phosphogypsum. Constr. Build. Mater. 184, 30, 68-75.

Gomaa E., Gheni A., ElGawady M. A., 2020. Repair of ordinary Portland cement concrete using ambient-cured alkali-activated concrete: Interfacial behavior. Cement Concrete Res. 129, 105968.

Hu X., Shi C.J., Yuan Q., Zhang J., Schutter G., 2020. Changes of pore structure and chloride content in cement pastes after pore solution expression. Cement Concrete Comp. 106, 103465.

Ines G.L., Ana F.J., Angel P., Donald E. M., 2010. Effect of calcium addition on N-A-S-H cementitious gels. J. Am. Ceram. Soc. 93, 1934-1940.

Ismail I., Bernal S. A., Provis J. L., Nicolas R. S., Hamdan S., Deventer van J. S.J., 2014. Modification of phase evolution in alkali-activated blast furnace slag by the incorporation of fly ash, Cem Concr Compos. 45, 125-135.

Izquierdo M., Querol X., Davidovits J., Antenucci D., Fernández-Pereira C., 2009. Coal fly ash-slag-based geopolymers: Microstructure and metal leaching. J. Hazard. Mater. 166, 561-566.

Kaboosi K., Emami K., 2009. Interaction of treated industrial wastewater and zeolite on compressive strength of plain concrete in different cement contents and curing ages. Case Studies in Construction Materials 11, e00308.

Kumar S., Kumar R., Mehrotra S.P., 2010. Influence of granulated blast furnace slag on the reaction, structure and properties of fly ash based geopolymer. J Mater Sci. 45(3),607-15.

Li L.B., Zhang H.M., Guo X.Y., Zhou X.M., Lu L.Ch., Cheng X., 2019a. Pore structure evolution and strength development of hardened cement paste with super low water-to-cement ratios. Constr. Build. Mater. 227, 117108.

Li Z.Zh., Zhang Y.Y., Zhao H.Y., Chen H.X., He R., 2019b. Structure characteristics and composition of hydration products of coal gasification slag mixed cement and lime. Constr. Build. Mater. 213, 265-274.

Li Z.X., Miao Z.Q., 2019. Primary air ratio affects coal utilization mode and NOx emission in lignite pulverized boiler. Energy 187, 116023.

Li D.D., Liu J.Zh., Wang Sh.N., Cheng J., 2020a. Study on coal water slurries prepared from coal chemical wastewater and their industrial application. Appl. Energ. 268, 114976.

Li P.R., Li W.G., Tao Yu, Qu F.l., Tam V. W. Y., 2020b. Investigation on early-age hydration, mechanical properties and microstructure of seawater sea sand cement mortar. Constr. Build. Mater.249, 118776.

Liu Zh.Q., You L.H., Xiong X.J., Wang Q., Wu X.H., 2019. Potential of the integration of coagulation and ozonation as a pretreatment of reverse osmosis concentrate from coal gasification wastewater reclamation. Chemosphere 222, 696-704.

Matjie R.H., Ward Z.Li.C.R., French D., 2008. Chemical composition of glass and crystalline phases in coarse coal gasification ash. Fuel 87, 857-869.

Nath S. K., Kumar S., 2019.Role of alkali concentration on reaction kinetics of fly ash geopolymerization. J. Non-Cryst. Solids 505, 241-251.

Provis J. L., 2018. Alkali-activated materials. Cem. Concr. Res. 114, 40-48.

Puertas F., Fernández-Jiménez A., 2003. Mineralogical and microstructural characterisation of alkali-activated fly ash/slag pastes. Cem. Concr. Compos. 25(3),287-292.

Qiao Ch.Y., Suraneni P., Weiss J., 2018. Flexural strength reduction of cement pastes exposed to CaCl2 solutions. Cement Concrete Comp. 86, 297-305.

Rashad A.M., Bai Y., Basheer P.A.M., Milestone N. B., Collier N. C., 2013. Hydration and properties of sodium sulfate activated slag. Cement Concrete Comp. 37, 20-29.

Rani R., Jain M. K., 2014. Status of ground water contamination by land filling of coal combustion residue: An overview. 3rd International Conference on Hydrology & Meteorology.

Sindhunata, Provis J.L., Lukey G.C., Xu H., Van Deventer J.SJ., 2008. Structural evolution of fly ash based geopolymers in alkaline environments. Ind Eng Chem Res. 47(9),2991-2999.

Shi D., Yao Y., Ye J.Y., Zhang W.Sh., 2019. Effects of seawater on mechanical properties, mineralogy and microstructure of calcium silicate slag-based alkali-activated materials. Constr. Build. Mater. 212, 569-577.

Tang Z., Li W.G., Hua Y., Zhou J.L., Tam V.W.Y., 2019. Review on designs and properties of multifunctional alkali-activated materials (AAMs). Constr. Build. Mater. 200, 474-489.

Tang, F. J，Glasser, F. P, 1988. Influence of Sulfate Source on Portland Cement Hydration. nce of Sulfate Source on Portland Cement Hydration. Adv. Cem. Res. 1(2), 67-74.

Walkley B., Nicolas R. S., Sani M.A., Rees G. J., Hanna J.V., Deventer J.S.J., Provis J. L., 2016. Phase evolution of C-(N)-A-S-H/N-A-S-H gel blends investigated via alkali-activation of synthetic calcium aluminosilicate precursors. Cem. Concr. Res. 89,120-135.

Wang W.D., Liu D.H., Tu Y.N., Jin L.Zh., Wang H., 2020. Enrichment of residual carbon in entrained-flow gasification coal fine slag by ultrasonic flotation. Fuel 278, 118195.

Wu S., Huang S., Wu Y., Gao G.S., 2015. Characteristics and catalytic actions of inorganic constituents from entrained-flow coal gasification slag. Energy Ins. 88, 93-103.

Xie K.Ch., Li W.Y., Zhao W., 2010. Coal chemical industry and its sustainable development in China. Energy 35, 4349-4355.

Xie B., Zhao H.D., Long H., Peng J.L., Liu R.Zh., 2019. 3D characteristics of pores in SiC particle preforms with different starchcontents by X-ray micro-computed tomography. Ceram. Int., 45, 23924-23933.

Xie J., Xin L., Hu X.M., Cheng W.M., Liu W.T., Wang Z.G., 2020. Technical application of safety and cleaner production technology by underground coal gasification in China. J. Clean. Prod. 250, 119487.

Yip C.K., Deventer J.S.J. van, 2003. Microanalysis of calcium silicate hydrate gel formed within a geopolymeric binder. J. Mater. Sci. 38, 3851-3860.

Yip C.K., Lukey G.C., Deventer J.S.J. van, 2005. The coexistence of geopolymeric gel and calcium silicate hydrate at the early stage of alkaline activation, Cem. Concr. Res. 35, 1683-1697.

Yu P., Kirkpatrick R.J., Poe B., McMillan P.F., Cong, X., 1999. Structure of calcium silicate hydrate (C-S-H): near, mid and far-infrared spectroscopy. J. Am. Ceram. Soc. 82, 742-748.

Yuan H., Yin H., Tang Y., Ge Z.F., He Ch., Li H.Zh., Bai Z.Q., Li W., 2014. The basis characteristics of gasification slag from texaco gasifier and shell gasifier. Appl. Mech. Mater. 675, 728-732.

Zdeb J., Howaniec N., Smoliński A., 2019. Utilization of Carbon Dioxide in Coal Gasification-An Experimental Study. Energies 12, 140.

Zhang R., Guo F.Y., Xia Y.Ch., Tan J.L., Tan J.L., Xing Y.W., Gui X.H., 2019. Recovering unburned carbon from gasification fly ash using saline water. Waste Manage. 98, 29-36.

Zhao X.L., Zeng C., Mao Y.Y., Li W.H., Peng Y., Wang T., 2010. The surface characteristics and reactivity of residual carbon in coal gasification slag. Energ. Fuel 24, 91-94.

Zhang D.W., Zhao K.F., Xie F.Zh., Li H., Wang D. M., 2020. Rheology and agglomerate structure of fresh geopolymer pastes with different Ms ratio of waterglass. Constr. Build. Mater. 250, 118881.